ACS Photonics

Article

pubs.acs.org/journal/apchd5

Graphene-Based Ultrathin Flat Lenses

Xiang-Tian Kong,[†] Ammar A. Khan,[‡,#] Piran R. Kidambi,[‡,#,¶] Sunan Deng,[§,#] Ali K. Yetisen,[∥] Bruno Dlubak,[‡] Pritesh Hiralal,[‡] Yunuen Montelongo,[‡] James Bowen,[⊥] Stéphane Xavier,[□] Kyle Jiang,[§] Gehan A. J. Amaratunga,[‡] Stephan Hofmann,[‡] Timothy D. Wilkinson,[‡] Qing Dai,*[,†] and Haider Butt*[,§]

[†]National Center for Nanoscience and Technology, Beijing 100190, China

[‡]Electrical Engineering Division, Department of Engineering, University of Cambridge, Cambridge CB3 0FA, U.K.

[§]School Mechanical Engineering, University of Birmingham, Birmingham B15 2TT, U.K.

[∥]Harvard Medical School and Wellman Center for Photomedicine, Massachusetts General Hospital 50 Blossom Street, Boston, Massachusetts 02114, United States

[⊥]School Chemical Engineering, University of Birmingham, Birmingham B15 2TT, U.K.

[□]Thales Research and Technology, 91767 Palaiseau, France

ABSTRACT: Flat lenses when compared to curved surface lenses have the advantages of being aberration free, and they offer a compact design necessary for a myriad of electro-optical applications. In this paper we present flat and ultrathin lenses based on graphene, the world's thinnest known material. Monolayers and multilayers of graphene were fabricated into Fresnel zones to produce Fresnel zone plates, which utilize the reflection and transmission properties of graphene for their operation. The working of the lenses and their performance in the visible and terahertz regimes were analyzed computationally. Experimental measurements were also performed to characterize the lens in the visible regime, and a good agreement was obtained with the simulations. This work demonstrates the principle of atom-thick graphene-based lenses, with perspectives for ultracompact integration.

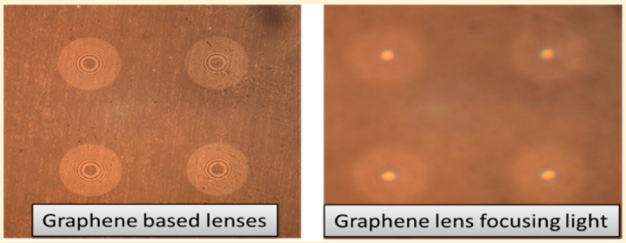

KEYWORDS: *graphene, thin lenses, Fresnel zone plates*

Fresnel zone plates are diffractive optical elements capable of focusing light. Unlike curved lenses, Fresnel zone plates are based on diffractive rings that deform the field.[1] When the rings are properly designed, it is possible to produce constructive interference at a given focal point. Binary intensity Fresnel zone plates use a flat surface with a set of radially symmetric rings, which alternate between opaque and transparent.[2] A Fresnel zone plate offers the possibility of designing high numerical aperture (NA) lens with low weight and small volume. It is, hence, widely used in silicon-based electronics with various applications, such as optical interconnects,[3] integrated optics,[4] beam focusing,[5,6] and maskless lithography systems.[7]

In this paper we demonstrate Fresnel zone plates (FZP)-based lenses made of graphene. Each graphene FZP lens has 24 zones, with a radius of about 50 μm. This is a major achievement in realizing efficient ultrathin lenses, which has the potential to improve the capabilities of compact optical systems, such as laser focusing for optical storage and fiber-optic communication.

A thin lens is defined as one with a thickness that is negligible compared to the focal length of the lens. Currently, lenses are not thin or flat enough to remove distortions, which limit imaging. Previously aberration was corrected by techniques such as aspheric shapes or multilens designs, resulting in heavy weight and extra space. Hence, it is very important to develop ultrathin lenses, and FZPs offer a suitable solution. From a theoretical perspective a diffractive element such as FZPs can achieve efficiencies close to 100% with diffraction-limited performance.[8,9] However, some physical constraints limit these possibilities. For instance, the relief of the diffractive plane is one of the sources of multiple aberrations in the focal plane.[10] Therefore, thin diffraction elements are desirable for the reduction of such distortions.

The ultrathin lens based on a 60 nm thick gold metasurface, fabricated by Federico Capasso et al.,[11] is considered to be a milestone to revolutionize consumer technology form factors. Here we report on the development of an ultrathin FZP lens using graphene on glass with a few nanometers thickness. Graphene is a single two-dimensional (2D) layer of carbon,[12] exhibiting a unique set of optoelectronic properties, in particular high optical transparency, low reflectance, and a high carrier mobility at room temperature.[13,14] This enables multiple functions of signal emitting, transmitting, modulating, and detection to be realized in one material[15] and makes graphene a promising choice for optoelectronic devices.[16] In the visible regime, the optical transmittance of single-layer

Received: June 4, 2014
Published: January 7, 2015

DOI: 10.1021/ph500197j
ACS Photonics 2015, 2, 200−207

graphene is frequency-independent and solely determined by the fine structure constant $\alpha = e^2/\hbar c$ (c is the speed of light): $T \equiv [1 + (2\pi G/c)]^{-2} \approx 1 - \pi\alpha \approx 0.977$, in which $G = e^2/4\hbar$ is the universal conductivity of graphene.[17] Compared with the transmittance, the reflectance of graphene under normal light incidence is relatively weak, with $R = 0.25\pi^2\alpha^2 T = 1.3 \times 10^{-4}$.

However, the opacity of multilayer graphene will increase linearly with the number of layers, N ($T \approx 1 - N\pi\alpha$). Unlike single-layer graphene, according to Skulason et al.,[18] few-layer graphene could have very high reflection contrast, indicating the possibility of making FZP lenses of graphene on glasses. For the FZP-based lenses the focal length f of the lens is related to the radii r of successive zone edges. By means of an approximation for large focal lengths, the radii of the rings can satisfy the equation $f/r_n = r_n/n\lambda$ (λ is the wavelength of light, n = 1, 2, 3, ...), and the radius of the nth zone (r_n) in a FZP lens is given by $r_n = n^{1/2}r_1$.[19] Setting the focal length to ~120 μm at an optical wavelength of 850 nm, the spacing and widths of the Fresnel zones were calculated with different n. Figure 1 shows the three-dimensional (3D) schematic diagram of the FZP geometry and its operation. The radius of the central zones was 10 μm, and the lens radius was about 49 μm.

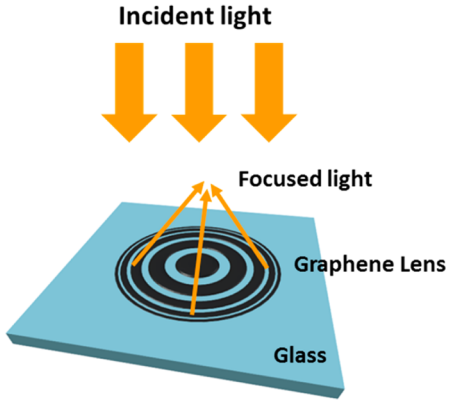

Figure 1. Schematic showing the geometry and reflection mode operation of the graphene Fresnel zone plate, with incident light from the top.

The graphene FZP was simulated by the finite element method, in which the lens is illuminated perpendicularly by a plane wave. The graphene is modeled as a material with equivalent permittivity given by $\varepsilon_g = i\sigma/\varepsilon_0\omega t_g$,[20] where ε_0 is the vacuum permittivity, ω is the angular frequency of light, t_g = 0.335 nm is the monolayer graphene thickness, and σ is the optical conductivity of graphene obtained from the Kubo formula.[21] In the Kubo formula, the conductivity is a function of the angular frequency ω, the Fermi level relative to the Dirac point E_F, the relaxation time τ, and temperature T. The relaxation time is obtained from $\tau = \mu E_F/ev_F^2$, where μ = 3000 cm^2/(V s) is the measured dc mobility,[22] e is the electron charge, and $v_F = 1 \times 10^6$ m/s is the Fermi velocity. The temperature is assumed to be 300 K. Note that the optical responses of graphene are not influenced by the sign of the Fermi level (p-doped or n-doped), owing to the linear electron dispersion relation of graphene. The thickness of the N-layer graphene is set to be equal to Nt_g in the simulations. The optical constant of the glass substrate is obtained from a Drude model fitted from the empirical data.[23] The Drude model of silica glass is given by $\varepsilon_{glass} = \varepsilon_\infty - \omega_0^2/(\omega^2 - \omega_r^2 + i\Gamma\omega)$, where ε_∞ = 2.11, ω_0 = 0.111 eV, ω_r = 0.132 eV, and Γ = 0.00882 eV. To obtain the scattered electromagnetic field ($\mathbf{E}_{sc}$ and $\mathbf{H}_{sc}$), the incident field is subtracted from the computed total field. Then, the scattered power flow distribution is calculated according to the Poynting theorem; $P_{sc} = \mathbf{E}_{sc} \times \mathbf{H}_{sc}^*$.

Figure 2a shows the computed power flow distribution of the reflected light by the FZP made by five-layer graphene, illuminated by light with 850 nm wavelength. The radius of the innermost graphene zone is 10 μm. Thus, the theoretical focal length is 117.6 μm. The horizontal and vertical cross-sectional lines at the focal point are shown in Figure 2b and c (solid lines), respectively. Here the Fermi level is assumed to be 0.1 eV. This simulation confirms the focusing of the reflected light of the graphene-based lens. In principle, the lensing effect of FZPs is determined by the reflection contrast between a silica glass surface and the zones covered by graphene. In the visible and near-infrared, the reflectance of a silica surface under perpendicular illumination from air is less than 3.5%. In contrast, the reflectance of a graphene-covered silica surface is much greater; see Figure 2d. For instance, the reflectance of 10-layer graphene on silica is 6.5%, which is nearly twice that of a bare silica surface. The reflection of Fresnel zones increases with an increasing number of graphene layers. Hence, the focusing efficiency, defined as the ratio of the focal intensity to the intensity of incident light, relies mainly on the number of layers of graphene for the incident light in the visible and near-infrared frequency range. For example, the dashed lines in Figure 2b and c show the cross sectional lines corresponding to a lens composed of 10-layer graphene. As shown, the intensity of reflected light at the focal point increases 2-fold when the layer number increases from 5 to 10.

Our graphene samples grown by chemical vapor deposition were hole-doped, and their Fermi level was less than ~0.25 eV.[22,24] The lens focusing effect mainly depends on graphene's permittivity,[25] so we studied both the real and imaginary part of five-layer graphene with different Fermi levels and different carrier mobility when illuminated with a 850 nm light source, as shown in Figure 3a,b. In the visible regime, the conductivity of graphene is dominated by the interband, and it is nearly constant due to Pauli blocking and the Fermi level lower than the interband onset ($2|E_F| < \hbar\omega$). Table 1 presents the focusing efficiency of the five-layer graphene lens under a Fermi level ranging from 0.05 to 0.6 eV. This Fermi level range is less than the interband onset value (0.73 eV for an incident wavelength of 850 nm), resulting in a nearly constant focusing efficiency of approximately 2.9% for the FZP made of five-layer graphene. Table 1 presents the focusing efficiency of the five-layer graphene lens under a Fermi level ranging from 0.05 to 0.6 eV. This Fermi level range is less than the interband onset value (0.73 eV for incident wavelength of 850 nm), resulting in a nearly constant focusing efficiency of approximately 2.9% for the FZP made of five-layer graphene.

At the same time, we may notice that there is a sharp peak in real permittivity and a razor edge in the imaginary permittivity at the interband onset Fermi level of 0.73 eV. So we compared the focal intensity with a carrier mobility of 10 000 cm^2/(V s) at Fermi levels of 0.1, 0.73, and 0.9 eV, as can be seen in Figure 3 c and d, which are focal intensity distributions in the vertical and horizontal cross sections, respectively. At the Fermi level of 0.73 eV, the focal intensity is much higher than the other two Fermi levels mainly due to the higher real permittivity part, with which more light will be reflected. The lowest focal

DOI: 10.1021/ph500197j
ACS Photonics 2015, 2, 200−207

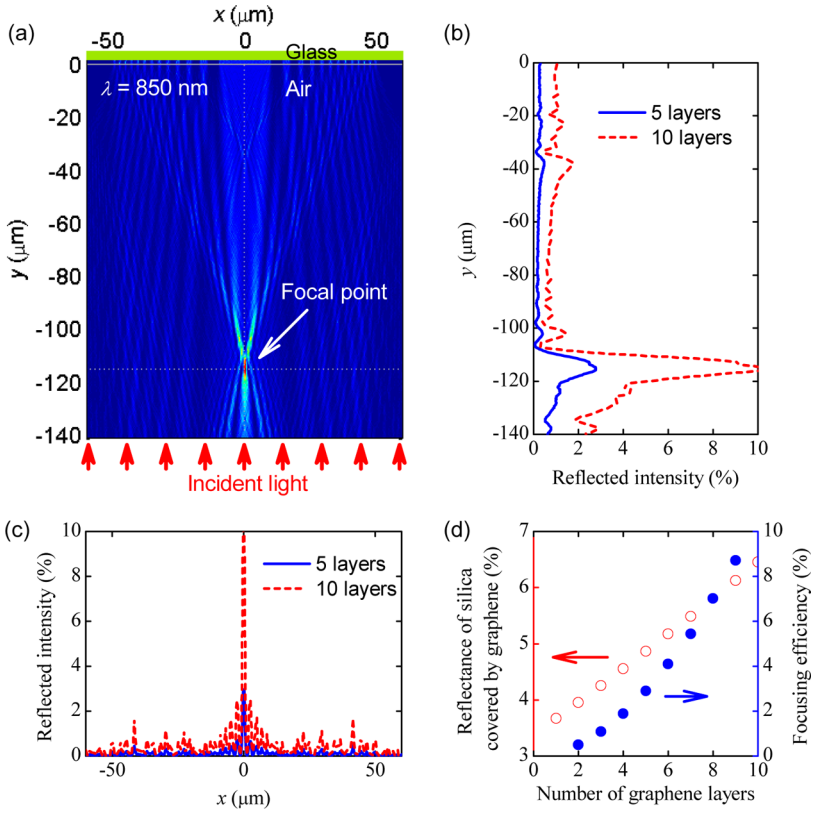

Figure 2. (a) Typical power flow distribution of the reflected light of the FZP. The lenses are located at $y = 0$ on a glass substrate ($y > 0$). Light of 850 nm wavelength is illuminated from the bottom boundaries of the computation domains. (b) Light intensity in terms of y extracted at $x = 0$. (c) Light intensity in terms of x at the focal plane. In (b) and (c), solid and dashed lines correspond to lenses with five- and 10-layer graphene, respectively. (d) Reflectance of silica surface covered by graphene and focusing efficiency of FZPs with respect to the number of graphene layers. The reflectance is calculated according to the Fresnel formula.

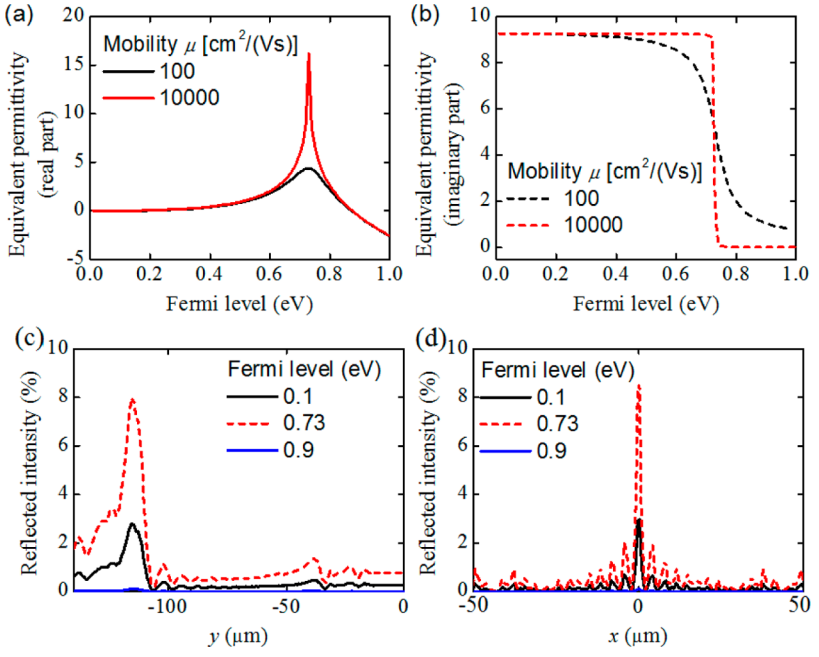

Figure 3. Properties of five-layer graphene and graphene Fresnel lens when incident light is 850 nm. (a) Real and imaginary part (b) of graphene permittivity at different carrier mobilities. Focal intensity distribution at different Fermi levels for graphene FZP with (c) $x = 0$ and (d) y at the focal plane.

intensity at the Fermi level of 0.9 eV is due to the lowest real permittivity.

According to the Kubo formula,[21] the conductivity of graphene is a function of the relaxation time τ, which is

DOI: 10.1021/ph500197j
ACS Photonics 2015, 2, 200−207

Table 1. Change in the Focal Intensity of the Lens with the Fermi Level[a]

Fermi level (eV)	focusing efficiency (%)
0.05	2.8924
0.1	2.8920
0.2	2.8894
0.3	2.8824
0.4	2.8696
0.5	2.8561
0.6	2.8860

[a]With mobility μ equal to 3000 $cm^2/(V\ s)$ for a lens with five-layer graphene under illumination of 850 nm wavelength.

proportional to the charge mobility. As a consequence, in general the lensing effect of FZPs varies with the charge mobility. In Figure 3a,b, we also studied the effect of carrier mobility on the permittivity of graphene. The red line represents a permittivity with a carrier mobility of 10 000 $cm^2/(V\ s)$, while the black line is a carrier mobility of 100 $cm^2/(V\ s)$. The carrier mobility causes a peak in the permittivity only near the interband onset (0.73 eV), while it shows no effect on permittivity for other values of the Fermi level.

As shown in Figure 4a, the focusing efficiency of the FZP made of five-layer graphene increases with increasing mobility for a fixed Fermi level (EF > 0.3 eV). However, the charge mobility has a negligibly small influence on the focused intensity distribution of the Fresnel zone plate in a broad range of 100−10 000 $cm^2/(V\ s)$ when the Fermi level of graphene is small (EF < 0.3 eV). Figure 4b shows the focused intensity plots across the focal plane at a Fermi level of 0.3 eV. With the charge mobility increasing from 100 to 10 000 $cm^2/(V\ s)$, no obvious change in the intensity profile can be observed. Figure 4c and d demonstrate the effect of carrier mobility on the lens focal intensity on interband onset. The mobility plays an important role at this special Fermi level, with higher carrier mobility leading to higher focal intensity.

On the basis of the simulation results mono-[22,24] and multilayer graphene[26,27] were synthesized by chemical vapor deposition (CVD), and Fresnel zone plates were fabricated by photolithography methods. The as-fabricated graphene lens array was characterized under an optical microscope. Figure 5a shows the lens array under the microscope, while Figure 5b shows the lens array focusing the light with excellent contrast. Figure 5c and d demonstrate the magnified version of a single graphene FZP lens and focal point along with the light intensity profile across the horizontal direction. It was clear from the intensity profiles that the focal point exhibits a good contrast. The experimental focal length of the graphene Fresnel lens is 175 ± 10 μm, with visible incident light. The simulations were performed for 850 nm and not visible light due to the large amount of computational memory required. However, the theoretically predicted focal length for the visible light (in the range 540.5−606 nm) was 175 ± 10 μm. Hence, experimental data correspond well with the expected value.

The lateral width of the experimentally measured focal spot is different from the simulations due to different light sources used. In the simulations, a monochromatic light source (wavelength 850 nm) was used to clearly demonstrate the lensing effect, whereas in the experiments a broad band white light source was used. Thus, the measured focus spot had a much wider area, as it is a net combination of many focal points made by different wavelengths.

The focusing efficiency of the lens is 6.57%, which is calculated from the ratio of light intensity at the focal point to the incident light intensity falling on the lenslet. The experimental focal efficiency corresponds well with the calculated value of 6.6% for nine-layer graphene, shown in

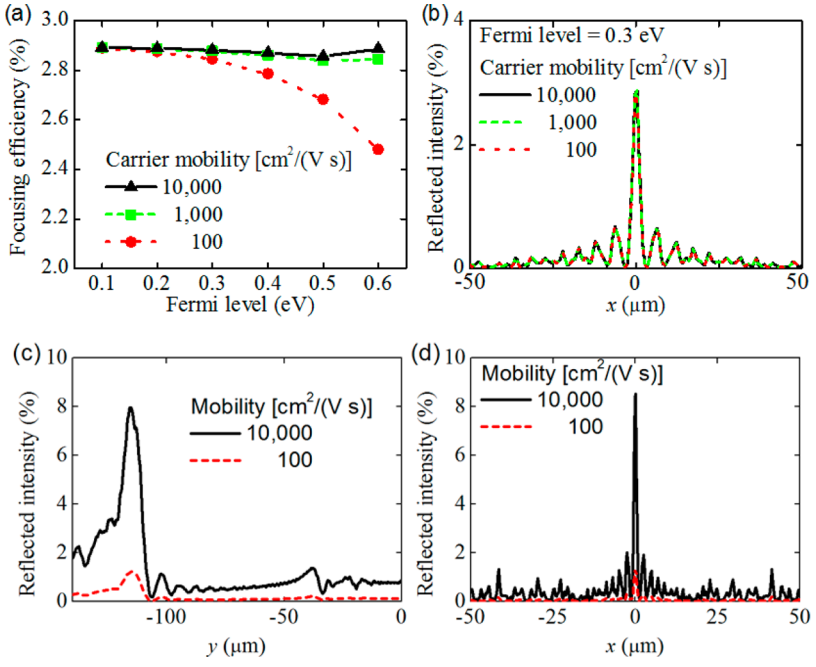

Figure 4. Effect of charge mobility on the lensing effect of graphene FZPs. (a) Focusing efficiency in terms of graphene Fermi level at charge mobilities of 10 000, 1000, and 100 $cm^2/(V\ s)$. (b) Reflected intensity at the focal plane with a Fermi level of 0.3 eV and carrier mobility of 10 000, 1000, and 100 $cm^2/(V\ s)$. (c, d) Focal intensity distribution with different carrier mobilities at an interband onset of 0.73 eV on horizontal and vertical cross sections, respectively. Here the FZP is made of five-layer graphene and illuminated by light of 850 nm wavelength.

DOI: 10.1021/ph500197j
ACS Photonics 2015, 2, 200−207

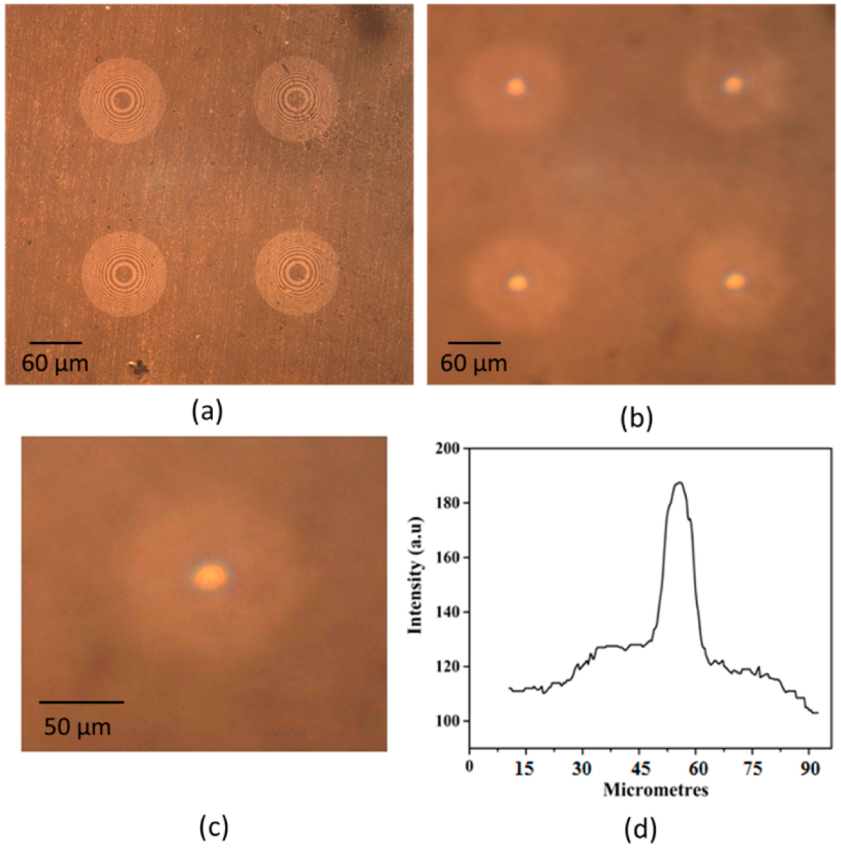

Figure 5. Graphene FZP lens array under reflection mode dark-field optical microscopy. (a) Optical image of the graphene FZP lens array. Each lenslet has 24 zones, and the radius of the center zone is 10 μm. (b) Graphene FZP showing the light focusing with excellent contrast. (c) Single FZP focusing spot. (d) Light intensity across the horizontal axis of the focal point in (c).

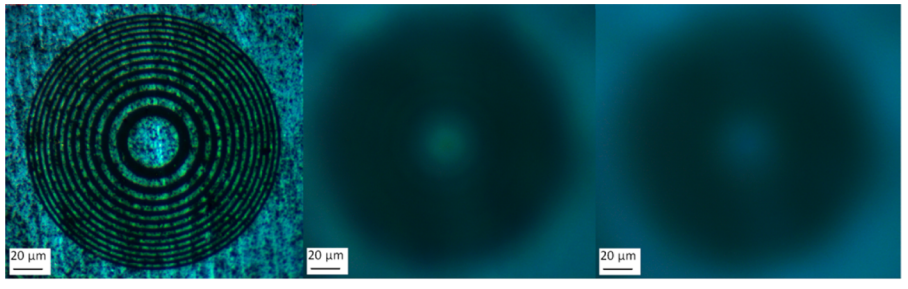

Figure 6. Single graphene FZP lenslet zoomed under an optical microscope. (a) Magnified single graphene lenslet. (b) Graphene lens working as a transmission lens. (c) Graphene lens working as a reflection lens.

Figure 2d (given that the graphene reflectance is constant across the visible range and 850 nm). The maximum efficiency reported for the ultrathin lens based on a 60 nm thick gold metasurface is approximately 1% for a wavelength of 1550 nm.[11] Also designing such metasurface lenses for the visible range will be a challenge due to the fine nanoscaled structures required. The graphene-based lenses offer more compactness and lower losses, are much easier to fabricate, and also offer tunability in the infrared range.

The lens arrays produced worked in both reflection and transmission mode of operation. In the transmission mode the focal point was produced within the glass substrate. Figure 6 shows the magnified version of a single graphene lens and focal points for two modes of operation. In Figure 6a, the dark zones are glass and the bright zones are graphene, which shows the good reflection optical contrast of few layer graphene on glass. By adjusting the focusing position of the microscope, we could get focusing spots both in glass (as show in Figure 6b, transmission mode) and in air (as show in Figure 6c, reflection mode).

To study the surface profile of the multilayered graphene lens, studies were carried out in an atomic force microscope (AFM). An AFM image of a single graphene FZP is shown in Figure 7. The bright spots in Figure 7a arise from the polymer residue postlithography and lead to artifacts in the AFM images, i.e., the black lines in Figure 7a. Figure 7b shows the information on the height distribution along the blue line. The Fresnel zones were clearly visible in the surface profile, and the average surface roughness was measured as 3.47 nm, which corresponds to approximately 10 layers of graphene. A few

DOI: 10.1021/ph500197j
ACS Photonics 2015, 2, 200−207

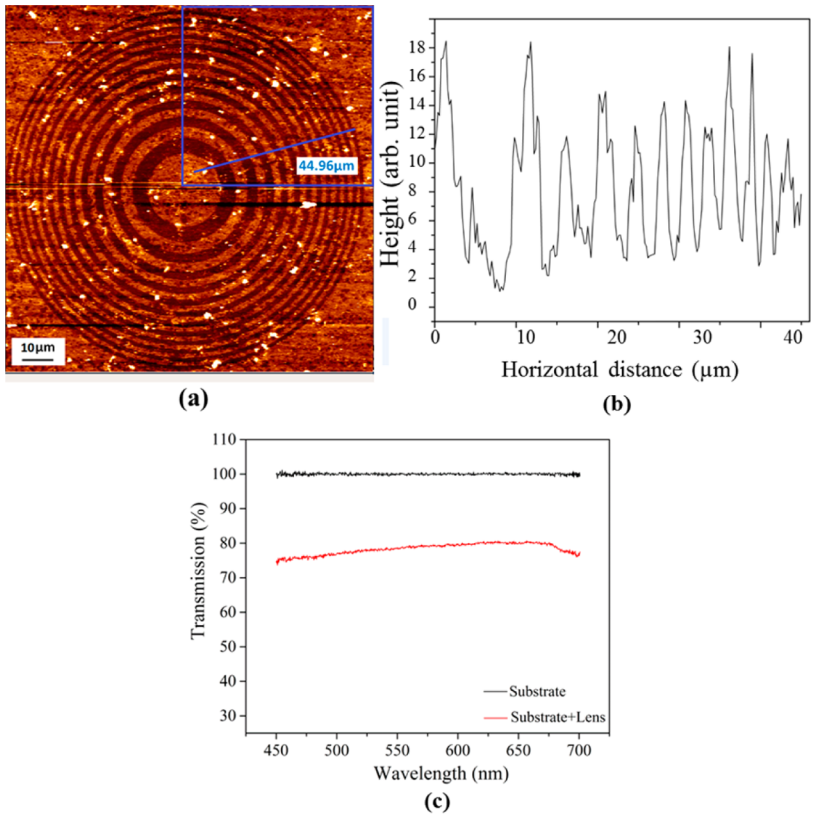

Figure 7. (a) AFM image of single graphene FZP. (b) Roughness distribution along the blue line. (c) Transmission spectrum for multilayered graphene used for producing the lens array.

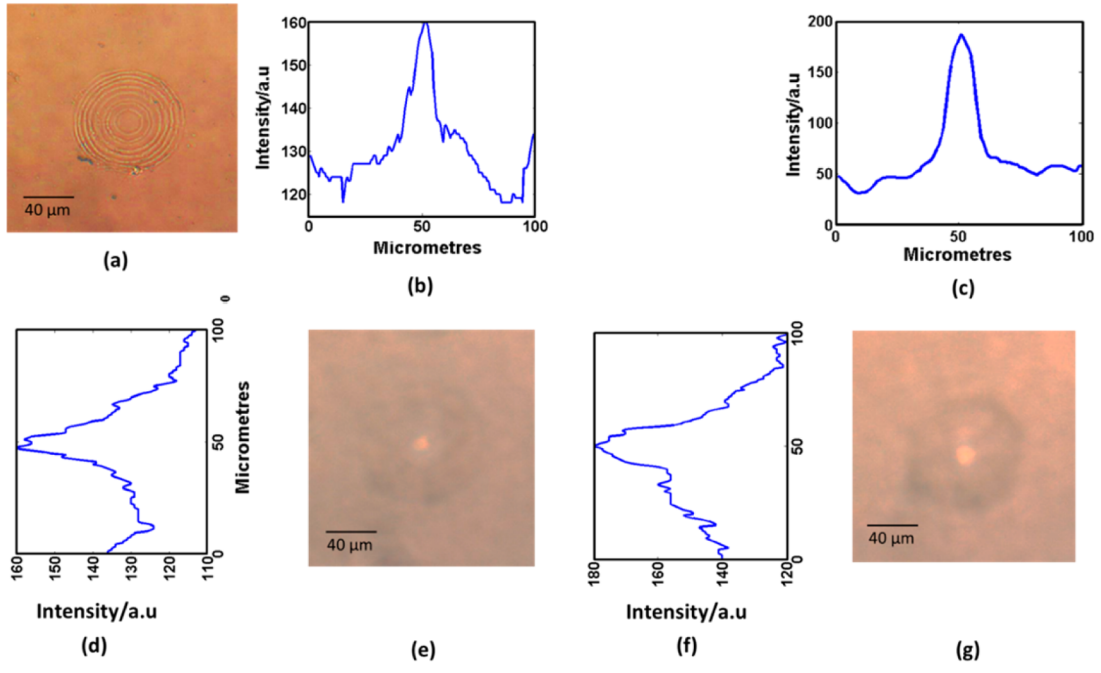

Figure 8. (a) Single-layer graphene Fresnel zone plate zoomed under an optical microscope. (e and g) The lens working under transmission mode and reflection mode, respectively. (b and c) Light intensity plots across the horizontal axis of transmission mode and reflection mode. (d and f) Light intensity plots across the vertical axis of transmission mode and reflection mode focal points.

peaks in the 8−10 nm range are observed due to the leftover polymer residues.

Optical transmission measurements were also performed for the multilayer graphene, which was used for making the FZPs. An Ocean Optics spectrometer connected to the optical microscope was used to measure the transmission spectra. Transmission spectra for glass and graphene on glass were measured as shown in Figure 7c. The results show that

DOI: 10.1021/ph500197j
ACS Photonics 2015, 2, 200−207

compared to the bare glass substrate, the graphene sample transmitted about 75−78% of the incident light. Theoretically, the transmission of 10-layer graphene is given by $T \approx 1 - N\pi\alpha \approx 77\%$. So the measured data are in good agreement with the theoretical calculation.

Finally to demonstrate the thinnest possible lens, a single layer of graphene was used. Samples consisting of monolayer graphene were patterned lithographically onto 0.7 mm thick glass using a Microtech laser writer (LW405, minimum resolution 0.7 μm) with a 405 nm laser. A positive resist (AZ5214) was used as an etch mask, spin coated at 4000 rpm, and dried at 100 °C for 1 min, resulting in a 1 μm thick resist film, which was subsequently patterned with the laser and developed. The sample was then ashed under oxygen plasma (100 W, 5−10 min) to etch the exposed graphene layers and subsequently washed thoroughly in acetone and 2-propanol to remove the remaining masking resist, leaving the patterned graphene surface. Figure 8a shows the single-layered graphene FZP lens under an optical microscope, while Figure 8e and g demonstrate the same, producing a focal point in the transmission and reflection modes of operation, respectively. The intensity profiles were also calculated across the focal points, which demonstrate good contrast.

Producing the thinnest possible flat lens using the novel graphene material is a next step toward achieving high resolution, low noise, and compact lenses for imaging applications. By increasing the widths of graphene-based lenses very high numerical apertures can also be achieved. Graphene is also being proposed as a transparent electrode for solar cells. By patterning it into the Fresnel zone plate-like geometries we demonstrated it can be simultaneously used as an optical concentrator. Moreover, as a future work graphene-based flat and compact lenses will be very useful in the terahertz range. In the terahertz frequency range, the conductivity (absorption) of graphene changes significantly with the Fermi level.[14,28] Hence, by controlling the Fermi levels (electronically) the performance of graphene-based lenses could be tuned.

In conclusion, we have developed ultrathin multi- and single-layer graphene-based Fresnel zone plate lenses on glass with nanoscale roughness. Through calculation and finite element modeling, the lenses were designed to operate in the optical regime. The lenses were fabricated by a lithography technique, and their focusing properties were characterized. The lenses were found to be thinner, more efficient, and easier to fabricate compared to the metasurface-based flat lenses. Hence the graphene lens arrays are highly promising as flat and ultrathin lenses, as they have the potential to revolutionize the design of compact optical systems, such as laser focusing for optical storage and fiber-optic communication.

AUTHOR INFORMATION

Corresponding Authors

*E-mail: daiq@nanoctr.cn. Tel: +86 10 82545720 (Q. Dai).
*E-mail: h.butt@bham.ac.uk. Tel: +44 121 4158623 (H. Butt).

Present Address

[¶]77 Massachusetts Avenue, Department of Mechanical Engineering, Massachusetts Institute of Technology, Cambridge, MA 02139-4307, United States.

Author Contributions

[#]A. A. Khan, P. R. Kidambi, and S. Deng contributed equally. The manuscript was written through contributions of all authors. All authors have given approval to the final version of the manuscript.

Notes

The authors declare no competing financial interest.

ACKNOWLEDGMENTS

P.R.K. acknowledges the Lindemann Trust Fellowship. H.B. would like to thank The Leverhulme Trust for the research funding. Q.D. is supported by Bureau of International Cooperation, Chinese Academy of Sciences (121D11KYSB20130013).

REFERENCES

(1) Aničin, B.; Babović, V.; Davidović, D. Fresnel lenses. *Am. J. Phys.* **1989**, *57*, 312.
(2) Rastani, K.; Marrakchi, A.; Habiby, S. F.; Hubbard, W. M.; Gilchrist, H.; Nahory, R. E. Binary phase Fresnel lenses for generation of two-dimensional beam arrays. *Appl. Opt.* **1991**, *30*, 1347−1354.
(3) Ferstl, M.; Frisch, A.-M. Static and dynamic Fresnel zone lenses for optical interconnections. *J. Mod. Opt.* **1996**, *43*, 1451−1462.
(4) Kodate, K.; Tokunaga, E.; Tatuno, Y.; Chen, J.; Kamiya, T. Efficient zone plate array accessor for optoelectronic integrated circuits: design and fabrication. *Appl. Opt.* **1990**, *29*, 5115−5119.
(5) Fallahi, M.; Kasunic, K. J.; Penner, S.; Nordman, O.; Peyghambarian, N. Design and fabrication of circular grating coupled distributed Bragg reflector lasers. *Opt. Eng.* **1998**, *37*, 1169−1174.
(6) Morgan, B.; Waits, C. M.; Krizmanic, J.; Ghodssi, R. Development of a deep silicon phase Fresnel lens using gray-scale lithography and deep reactive ion etching. *J. Microelectromech. Syst.* **2004**, *13*, 113−120.
(7) Carter, D. J. D.; Gil, D.; Menon, R.; Mondol, M. K.; Smith, H. I.; Anderson, E. H. Maskless, parallel patterning with zone-plate array lithography. *J. Vac. Sci. Technol. B* **1999**, *17*, 3449−3452.
(8) Perry, M.; Shannon, C.; Shults, E.; Boyd, R.; Britten, J.; Decker, D.; Shore, B. High-efficiency multilayer dielectric diffraction gratings. *Opt. Lett.* **1995**, *20*, 940−942.
(9) Menon, R.; Gil, D.; Smith, H. I. Experimental characterization of focusing by high-numerical-aperture zone plates. *JOSA A* **2006**, *23*, 567−571.
(10) Hessler, T.; Rossi, M.; Kunz, R. E.; Gale, M. T. Analysis and optimization of fabrication of continuous-relief diffractive optical elements. *Appl. Opt.* **1998**, *37*, 4069−4079.
(11) Aieta, F.; Genevet, P.; Kats, M. A.; Yu, N.; Blanchard, R.; Gaburro, Z.; Capasso, F. Aberration-free ultrathin flat lenses and axicons at telecom wavelengths based on plasmonic metasurfaces. *Nano Lett.* **2012**, *12*, 4932−4936.
(12) Geim, A. K.; Novoselov, K. S. The rise of graphene. *Nat. Mater.* **2007**, *6*, 183−191.
(13) Butt, H.; Kidambi, P. R.; Dlubak, B.; Montelongo, Y.; Palani, A.; Amaratunga, G. A.; Hofmann, S.; Wilkinson, T. D. Visible diffraction from graphene and its application in holograms. *Adv. Opt. Mater.* **2013**, *1*, 869−874.
(14) Degl'Innocenti, R.; Jessop, D. S.; Shah, Y. D.; Sibik, J.; Zeitler, J. A.; Kidambi, P. R.; Hofmann, S.; Beere, H. E.; Ritchie, D. A. Low-bias terahertz amplitude modulator based on split-ring resonators and graphene. *ACS Nano* **2014**, *8*, 2548−2554.
(15) Bao, Q.; Loh, K. P. Graphene photonics, plasmonics, and broadband optoelectronic devices. *ACS Nano* **2012**, *6*, 3677−3694.
(16) Cooper, D. R.; D'Anjou, B.; Ghattamaneni, N.; Harack, B.; Hilke, M.; Horth, A.; Majlis, N.; Massicotte, M.; Vandsburger, L.; Whiteway, E. Experimental review of graphene. *Condens. Mater. Phys.* **2012**, 2012.
(17) Nair, R.; Blake, P.; Grigorenko, A.; Novoselov, K.; Booth, T.; Stauber, T.; Peres, N.; Geim, A. Fine structure constant defines visual transparency of graphene. *Science* **2008**, *320*, 1308−1308.
(18) Skulason, H.; Gaskell, P.; Szkopek, T. Optical reflection and transmission properties of exfoliated graphite from a graphene

DOI: 10.1021/ph500197j
ACS Photonics 2015, 2, 200−207

monolayer to several hundred graphene layers. *Nanotechnology* **2010**, *21*, 295709.
(19) Fan, Y.-H.; Ren, H.; Wu, S.-T. Switchable Fresnel lens using polymer-stabilized liquid crystals. *Opt. Express* **2003**, *11*, 3080−3086.
(20) Vakil, A.; Engheta, N. Transformation optics using graphene. *Science* **2011**, *332*, 1291−1294.
(21) Gusynin, V.; Sharapov, S.; Carbotte, J. Magneto-optical conductivity in graphene. *J. Phys.: Condens. Mater.* **2007**, *19*, 026222.
(22) Kidambi, P. R.; Ducati, C.; Dlubak, B.; Gardiner, D.; Weatherup, R. S.; Martin, M.-B.; Seneor, P.; Coles, H.; Hofmann, S. The parameter space of graphene chemical vapor deposition on polycrystalline Cu. *J. Phys. Chem. C* **2012**, *116*, 22492−22501.
(23) Palik, E. D. *Handbook of Optical Constants of Solids*: Index. Access online via Elsevier, 1998.
(24) Kidambi, P. R.; Bayer, B. C.; Blume, R.; Wang, Z.-J.; Baehtz, C.; Weatherup, R. S.; Willinger, M.-G.; Schloegl, R.; Hofmann, S. Observing graphene grow: catalyst−graphene interactions during scalable graphene growth on polycrystalline copper. *Nano Lett.* **2013**, *13*, 4769−4778.
(25) Deng, S.; Yetisen, A. K.; Jiang, K.; Butt, H. Computational modelling of a graphene Fresnel lens on different substrates. *RSC Adv.* **2014**, *4*, 30050−30058.
(26) Kidambi, P. R.; Bayer, B. C.; Weatherup, R. S.; Ochs, R.; Ducati, C.; Szabó, D. V.; Hofmann, S. Hafnia nanoparticles−a model system for graphene growth on a dielectric. *Phys. Status Solidi (RRL)* **2011**, *5*, 341−343.
(27) Xi, K.; Kidambi, P. R.; Chen, R.; Gao, C.; Peng, X.; Ducati, C.; Hofmann, S.; Kumar, R. V. Binder free three-dimensional sulphur/few-layer graphene foam cathode with enhanced high-rate capability for rechargeable lithium sulphur batteries. *Nanoscale* **2014**, *6*, 5746−5753.
(28) Badhwar, S.; Sibik, J.; Kidambi, P. R.; Beere, H. E.; Zeitler, J. A.; Hofmann, S.; Ritchie, D. A. Intrinsic terahertz plasmon signatures in chemical vapour deposited graphene. *Appl. Phys. Lett.* **2013**, *103*, 121110.

DOI: 10.1021/ph500197j
ACS Photonics 2015, 2, 200−207